

Hydrodynamics of Fermi arcs: bulk flow and surface collective modes

E. V. Gorbar^{1,2} V. A. Miransky³ I. A. Shovkovy^{4,5} and P. O. Sukhachov³

¹*Department of Physics, Taras Shevchenko National Kiev University, Kiev, 03680, Ukraine*

²*Bogolyubov Institute for Theoretical Physics, Kiev, 03680, Ukraine*

³*Department of Applied Mathematics, Western University, London, Ontario, Canada N6A 5B7*

⁴*College of Integrative Sciences and Arts, Arizona State University, Mesa, Arizona 85212, USA*

⁵*Department of Physics, Arizona State University, Tempe, Arizona 85287, USA*

(Dated: January 1, 2019)

The hydrodynamic description of the Fermi arc surface states is proposed. In view of the strong suppression of scattering on impurities, the hydrodynamic regime for Fermi arc states should be, in principle, plausible. By using the kinetic theory, the Fermi arc hydrodynamics is derived and the corresponding effects on the bulk flow and surface collective modes are studied. For the bulk flow, the key effect of the proposed Fermi arc hydrodynamics is the modification of the corresponding boundary conditions. In a slab geometry, it is shown that, depending on the transfer rates between the surface and bulk, the hydrodynamic flow of the electron fluid inside the slab could be significantly altered and even enhanced near the surfaces. As to the spectrum of the surface collective modes, in agreement with earlier studies, it is found that the Fermi arcs allow for an additional gapless spectrum branch and a strong anisotropy of the surface plasmon dispersion relations in the momentum space. The gapped modes are characterized only by closed elliptic constant-frequency contours.

I. INTRODUCTION

Weyl semimetals are materials with a relativisticlike energy spectrum in the vicinity of isolated Weyl nodes in the Brillouin zone. (For recent reviews on Weyl semimetals, see Refs. [1–3].) The nodes have nonzero topological charges with the monopolelike Berry curvature [4] and always occur in pairs of opposite chirality [5, 6]. In each pair, the Weyl nodes can be separated in energy and/or momentum, which indicates breaking of the parity-inversion (PI) and/or time-reversal (TR) symmetries, respectively. The nontrivial topology and the relativisticlike nature of quasiparticles also affect the transport properties of Weyl semimetals, e.g., leading to a negative longitudinal magnetoresistivity that was first predicted in Ref. [7]. (For recent reviews of the transport phenomena, see Refs. [8–10].)

The nontrivial bulk topology of Weyl semimetals is also reflected in unusual surface states known as the Fermi arcs [11]. Unlike surface states in ordinary materials, the Fermi arcs form open segments in momentum space that connect Weyl nodes of opposite chirality [11, 12]. The surface states in Weyl semimetals were observed via the angle resolved photoemission spectroscopy [13–19], as well as reconfirmed by the observation of the quasiparticle interference patterns [20–23]. It is important to note that the energy dispersion of the Fermi arc states is effectively one-dimensional (see, e.g., Ref. [24]). This may suggest that the corresponding transport is similar to that of the one-dimensional chiral fermions and should be nondissipative. However, as we showed in Ref. [25], the Fermi arc transport is, in fact, dissipative because of the scattering between the surface and bulk states in Weyl semimetals. The dissolution of Fermi arcs in the presence of strong disorder was also confirmed numerically in Refs. [26, 27].

Electronic collective excitations provide additional powerful probes of the nontrivial properties of Weyl semimetals. The topology is imprinted, for example, in anomalous helicons [28], surface plasmon polaritons [29, 30], chiral magnetic plasmons [31–33], etc. The effect of the Fermi arcs on the surface plasmons was studied in Refs. [34–36]. The authors of Ref. [34] employed a simple phenomenological model valid in the long-wavelength limit. The hybridization of the Fermi arc and conventional surface plasmons is controlled via the anomalous Hall conductivity and a phenomenologically included Drude weight. Further, the surface plasmon excitation spectrum in Weyl semimetal within the random phase approximation was determined in Ref. [36]. The treatment of the surface plasmons in Ref. [35] is more sophisticated and is based on the direct quantum-mechanical calculations. Despite the difference in their approaches, studies in Refs. [34, 35] predict the open hyperbolic constant-frequency contours for the surface plasmons. The nontrivial patterns of the surface plasmons can be measured by the scattering-type near-field optical spectroscopy (for a recent review, see Ref. [37]) as well as the momentum-resolved electron energy loss spectroscopy (see e.g., Ref. [38] and the references therein). Experimentally, the electron energy loss in Weyl semimetals was recently studied in Ref. [39].

Since Weyl semimetals are typically characterized by low impurity scattering rates, one might suggest that a hydrodynamic regime of electron transport could be realized in such materials. Originally, the possibility of such a regime for charge carriers in sufficiently clean solids was discussed in the pioneering papers by Gurzhi [40, 41]. Electron hydrodynamics requires that the electron-electron scattering rate dominates over the electron-impurity and electron-phonon ones. Recently, such a regime was experimentally confirmed in the Weyl semimetal tungsten diphosphide

(WP₂) [42], where the characteristic quadratic dependence of the electrical resistivity on the cross section of the wire as well as a strong violation of the Wiedemann–Franz law were observed.

Theoretically, the nontrivial topological properties of Weyl semimetals, connected with the energy and momentum separations between Weyl nodes, are taken into account in the recently proposed framework of consistent hydrodynamics [43]. The latter includes several types of Chern–Simons contributions in the electric current and charge densities that affect not only the electron transport in Weyl semimetals [44, 45], but also their various collective excitations [43, 46]. It is natural to ask, therefore, whether the hydrodynamic regime could be also realized for the Fermi arc electrons and, if so, how it would affect the bulk electron fluid.

A low sensitivity of the surface Fermi arc states to disorder makes them promising candidates to sustain a *surface electron fluid* in Weyl semimetals. If this is indeed the case, the Fermi arcs could realize not only the “Fermi level plumbing” [12], but act as true aqueducts for the surface electron fluid. Because of the inevitable surface-bulk transitions and interactions, of course, such a surface electron fluid should be necessarily coupled to the bulk one.

In this study, we derive the hydrodynamic equations for the surface Fermi arc states from the kinetic theory and phenomenologically describe the corresponding surface-bulk coupling. Our principal finding is that the Fermi arc electron liquid modifies the boundary conditions for the bulk one. Depending on the coupling parameters, the bulk flow in a slab of finite thickness could be noticeably altered and even enhanced near the surface. In addition, we study the surface collective modes in the hydrodynamic approximation. In agreement with the earlier studies [34–36], the presence of the Fermi arcs is manifested in a strongly anisotropic dispersion relation of the surface plasmons. Additionally, we find that while the constant-frequency contours of the surface modes are given only by the elongated ellipses, the open hyperbolic contours correspond to the bulk modes hybridized with the surface excitations similarly to the usual semi-infinite plasma [47]. Finally, there is also a gapless surface mode, which is related exclusively to the Fermi arcs. While such a mode resembles a conventional surface acoustic plasmon [48], which also has a linear dispersion relation, the Fermi arc mode is different and its frequency is determined by the surface dispersion relation.

Our paper is organized as follows. In Sec. II, we introduce the phenomenological hydrodynamic model of the Fermi arcs and discuss the coupling of the surface and bulk electron fluids. The explicit realization of coupling is given and the effects of the surface states on the hydrodynamic flow are studied in Sec. III. Sec. IV is devoted to the investigation of the surface collective modes in the hydrodynamic approximation. Our results are discussed and summarized in Sec. V. Technical details, including the derivation of the Fermi arc hydrodynamic equations and some auxiliary formulas are given in Appendices A and B, respectively. Throughout this paper, we set the Boltzmann constant $k_B = 1$.

II. MODEL

In order to derive the hydrodynamic equations for the Fermi arc quasiparticles, we start from the kinetic theory. As usual [49, 50], the Euler equation is obtained by calculating the appropriate moments of the kinetic equation. In the presence of the electric field \mathbf{E} , the latter reads

$$\partial_t f^{(\text{FA})} - e\mathbf{E} \cdot \partial_{\mathbf{p}} f^{(\text{FA})} + \mathbf{v}_p^{(\text{FA})} \cdot \nabla f^{(\text{FA})} = I_{\text{coll}}^{(\text{FA})}, \quad (1)$$

where $-e$ is the electron charge, $\mathbf{p} = (p_x, p_z)$ is the two-dimensional momentum of the surface quasiparticles, and $I_{\text{coll}}^{(\text{FA})}$ denotes the collision integral, whose effects on the Fermi arcs will be discussed later. In the hydrodynamic regime, the distribution function describes local equilibrium, i.e.,

$$f^{(\text{FA})} = \delta(y - y_s) \frac{1}{1 + \exp\left(\frac{\epsilon_p^{(\text{FA})} - (\mathbf{u}^{(\text{FA})} \cdot \mathbf{p}) - \mu}{T}\right)}, \quad (2)$$

where y_s denotes the surface coordinate, $s = \pm$ labels the bottom and top surfaces, respectively, $\mathbf{u}^{(\text{FA})}$ is the Fermi arcs fluid velocity, μ is the electric chemical potential, and T is temperature. For a slab of finite thickness L_y , the coordinates of the top and bottom surfaces will be fixed at $y_- = L_y$ and $y_+ = 0$, respectively. Here, for simplicity, we assume that the Fermi arcs are strongly localized at the sample’s boundaries and, therefore, the dependence of the distribution function on the transverse coordinate can be modeled by the δ -functions.

Further, we assume that the Weyl semimetal has a broken TR symmetry and contains two Weyl nodes separated by $2b$ along the z direction in momentum space. Then, by making use of a simple model (see, e.g., Ref. [24]), we find that the dispersion relation for the Fermi arc states reads

$$\epsilon_p^{(\text{FA})} = s v_F p_x, \quad (3)$$

where v_F is the Fermi velocity. It should be noted that the quasiparticle velocity for the Fermi arc quasiparticles

$$\mathbf{v}_p^{(\text{FA})} = \partial_{\mathbf{p}} \epsilon_p^{(\text{FA})} = sv_F \hat{\mathbf{x}} \quad (4)$$

is parallel to the x axis. Therefore, it is reasonable to assume that $\mathbf{u}^{(\text{FA})}$ also points along the x direction. In other words, there should be no hydrodynamic flow due to the Fermi arcs in the z direction. Of course, the same is true for the surface electric current, which can only flow along $\mathbf{v}_p^{(\text{FA})}$, see Eq. (A15) in Appendix A 2. We note that this is qualitatively different from the setup in Ref. [34], where a diffusive surface transport along the z direction was allowed.

The derivation of the hydrodynamic equation for the Fermi arc electron fluid is given in Appendix A. In the inviscid limit, which might be justified in the case of relatively small electron-electron collision times, the Euler equation for the surface hydrodynamic velocity reads

$$(\partial_t + sv_F \partial_x) \frac{sw^{(\text{FA})}}{v_F} \left(1 + 2 \frac{u_x^{(\text{FA})}}{sv_F} \right) + en^{(\text{FA})} \left(1 + \frac{u_x^{(\text{FA})}}{sv_F} \right) E_x = I_s^{(\text{FA})}, \quad (5)$$

where $I_s^{(\text{FA})}$ stems from the collision integral $I_{\text{coll}}^{(\text{FA})}$ and describes the surface-bulk transitions. We also introduced the following notations for the enthalpy and the fermion number density of the Fermi arc states in equilibrium:

$$w^{(\text{FA})} = \frac{b}{4\pi^2 v_F \hbar} \left(\mu^2 + \frac{\pi^2 T^2}{3} \right), \quad (6)$$

$$n^{(\text{FA})} = \frac{\mu b}{2\pi^2 v_F \hbar}. \quad (7)$$

[For the derivation of the Fermi arc charge density, see Eq. (A14) in Appendix A 2.]

Now, let us briefly discuss the bulk hydrodynamics. In the absence of external magnetic fields and vorticity, the Navier–Stokes equation for the quasiparticles in a Weyl semimetal reads [44, 51]

$$\partial_t \frac{w}{v_F^2} \mathbf{u} - \eta \Delta \mathbf{u} - \left(\zeta + \frac{\eta}{3} \right) \nabla (\nabla \cdot \mathbf{u}) + \nabla P + en \mathbf{E} + \frac{w}{v_F^2 \tau} \mathbf{u} = \mathbf{I}_{\text{surf}}. \quad (8)$$

Here $w = \epsilon + P$ is the bulk enthalpy, ϵ is the bulk energy density, P is the pressure, \mathbf{u} is the bulk fluid velocity, n is the bulk fermion number density, η and ζ are the shear and bulk dynamic viscosities, respectively. Note that, in the global equilibrium state without background electromagnetic fields and with vanishing fluid velocity, the energy density, the pressure, and the fermion number density take the following explicit forms:

$$\epsilon = \frac{15\mu^4 + 30\pi^2 T^2 \mu^2 + 7\pi^4 T^4}{60\pi^2 \hbar^3 v_F^3}, \quad (9)$$

$$P = \frac{\epsilon}{3}, \quad (10)$$

$$n = \frac{\mu (\mu^2 + \pi^2 T^2)}{3\pi^2 \hbar^3 v_F^3}. \quad (11)$$

In relativistic-like systems, the shear and bulk viscosities can be estimated as $\eta = w \tau_{ee} / 4$ (see, e.g., Refs. [42, 52]) and $\zeta \approx 0$ [49]. In our study, we use the scattering time $\tau_{ee} = \hbar/T$, which is consistent with the experimental findings in Ref. [42].

Compared to the conventional Navier–Stokes equation [53], Eq. (8) contains a few additional contributions. While the penultimate term on the left-hand side accounts for the charged nature of the electron fluid and describes the electrical force, the term inversely proportional to the relaxation time τ is a hallmark feature of the solid-state hydrodynamics [41]. It comes from the electron scattering on phonons and impurities and, as is clear from its explicit dependence on the fluid velocity, it breaks the Galilean invariance. As for the term on the right-hand side of Eq. (8), it describes the transfer of momentum between the surface and bulk fluids. By taking into account that the Fermi arcs are localized on the surface, it can be modeled as follows:

$$\mathbf{I}_{\text{surf}} = - \sum_{s=\pm} \delta(y - y_s) I_s^{(\text{FA})} \hat{\mathbf{x}}, \quad (12)$$

where $y_+ = 0$ and $y_- = L_y$ are the coordinates of the two slab surfaces. The inclusion of the source term in Eq. (8) implies that the boundary conditions (BCs) for the electron fluid should be modified. Instead of the usual free-surface BCs, the fluid velocity and its derivatives should satisfy the following BCs at $y = y_s$:

$$\eta \partial_y u_x(y_s) + \left(\zeta + \frac{\eta}{3} \right) \partial_x u_y(y_s) = s I_s^{(\text{FA})}. \quad (13)$$

Additionally, the normal components of the electron fluid velocity should vanish on both surfaces, i.e.,

$$u_y(y_s) = 0. \quad (14)$$

In order to illustrate the nontrivial effects of the Fermi arcs, we will also consider the benchmark case, where the chiral shift is absent or directed normal to the surfaces of the slab. In such a simplified setup, there are no Fermi arc surface states and the BCs for the bulk fluid velocity take the standard no-slip form, i.e.,

$$u_x(y_s) = 0 \quad (15)$$

or the free-surface form, i.e.,

$$\partial_y u_x(y_s) = 0. \quad (16)$$

Since the Fermi arc fluid velocity affects only the x component of the bulk flow, the z component of the fluid velocity always satisfies the standard no-slip or free-surface BCs similar to those in Eqs. (15) or (16).

It is worth noting that the Navier-Stokes equation should be amended by the energy conservation relation as well as the electric current continuity relation. While the latter has a profound effect on both the charge transport and collective excitations, the former is important only for the thermoelectric effects and can usually be neglected in electron transport [53]. In general, however, the effect of the energy conservation on the electron hydrodynamics may become important when the fluid velocity is not small compared to the speed of sound v_s (note that v_s is close to $v_F/\sqrt{3}$ in relativisticlike systems). Therefore, in what follows, we will assume that $|\mathbf{u}| \ll v_s$ and the energy conservation relation can be ignored.

The electric current continuity relations for the surface and bulk states read

$$\partial_t \rho_s^{(\text{FA})} + \nabla_{\perp} \cdot \mathbf{J}_s^{(\text{FA})} = Q_s^{(\text{FA})}, \quad (17)$$

$$\partial_t \rho + \nabla \cdot \mathbf{J} = - \sum_{s=\pm} \delta(y - y_s) Q_s^{(\text{FA})}, \quad (18)$$

respectively. Here $Q_s^{(\text{FA})}$ describes the electric charge transfer between the bulk and surface states of the semimetal. Further, $\rho_s^{(\text{FA})} = -en^{(\text{FA})} \left(1 + su_x^{(\text{FA})}/v_F\right)$ is the surface electric charge density and $\rho = -en$ is the bulk one. The surface and bulk electric currents are given by

$$\mathbf{J}_s^{(\text{FA})} = sv_F \rho_s^{(\text{FA})} \hat{\mathbf{x}}, \quad (19)$$

$$\mathbf{J} = -en\mathbf{u} + \sigma\mathbf{E} + \frac{e^2 [\mathbf{b} \times \mathbf{E}]}{2\pi^2 \hbar}, \quad (20)$$

respectively. The explicit expressions for the Fermi arc charge and current densities are derived in Appendix A 2. Note that the expression for the bulk current (20) includes the intrinsic conductivity σ , which was discussed in the holographic approach in Refs. [54–58]. While σ is important for a correct description of the normal flow in the presence of a nonzero chiral shift [44], it plays no role in the longitudinal flow. The last term in Eq. (20) corresponds to the anomalous Hall effect [59–65], where $\mathbf{b} = b\hat{\mathbf{z}}$ is the chiral shift.

By integrating Eq. (18) in the vicinity of the surfaces, we obtain the following boundary condition for the normal component of the bulk current:

$$J_y(y_s) = -sQ_s^{(\text{FA})}. \quad (21)$$

Formally, this implies that, because of the transitions between the surface and bulk states, the normal component of the bulk current does not vanish on the surface.

Before concluding this section, it is instructive to sum up the general features of the surface and bulk flows, as well as to reiterate the critical role that the BCs play in their interplay. The surface $u_x^{(\text{FA})}$ and bulk \mathbf{u} fluid velocities are determined by the hydrodynamic equations (5) and (8), respectively. The bulk equation should be also supplemented by the appropriate BCs for the normal component of the fluid velocity, see Eq. (14), as well as the BCs for the tangential components, see Eqs. (13) or, in the absence of the Fermi arcs, Eqs. (15) and (16). In addition, as we will see below, the study of the longitudinal flow requires specifying either the Fermi arc fluid velocity at some contacts or an explicit form of the transfer terms. In our study, we use the latter option that allows a self-consistent determination of the surface fluid velocity as well as the bulk flow. As for the collective excitations, the use of the continuity relations (17) and (18) will be needed in order to determine the evolution of the electric charge. In this connection, it should be emphasized that, because of the presence of the surface states, the normal component of the bulk electric current (21) does not vanish at the boundary.

III. HYDRODYNAMIC FLOW

In this section, we investigate a steady hydrodynamic flow in a slab of finite width in the y direction (and infinite in the x and z directions). Without loss of generality, we will assume that a uniform background electric field is applied in the x direction. Incidentally, this is same setup as we used in Ref. [44], where, however, the effects of the Fermi arcs were not taken into account.

Since the bulk electron fluid couples to the surface states, the transfer term on the right-hand side in Eq. (5) plays an important role in the hydrodynamic flow. We model it as follows:

$$I^{(\text{FA})} = -\frac{w^{(\text{FA})} u_x^{(\text{FA})}}{v_F^2 \tau_{sb}} + \frac{\alpha w u_x(y_s)}{v_F}. \quad (22)$$

Here the first term describes the transitions from the surface to the bulk with the rate determined by the relaxation time τ_{sb} . The second term corresponds to the inflow from the bulk to the surface, where the rate is parameterized by a small numerical coefficient α . [For the derivation of the transfer terms, see Eqs. (A12) and (A13) in Appendix A 2.] Recall that the surfaces of the slab are located at $y_+ = 0$ and $y_- = L_y$. Here we assume that the slab is sufficiently thick so that the interaction between the Fermi arcs on the opposite surfaces is negligible and the arcs could be considered as independent. At the same time, the thickness should be small enough in order for the surface flow to have a noticeable effect on the net hydrodynamic flow.

Taking into account that the right-hand sides of the bulk Navier-Stokes (8) and continuity (18) equations are nonzero only at the surfaces of the slab, it is reasonable to take them into account only via the BCs. In particular, we will use Eq. (13) for the velocity on the surface and Eq. (21) for the normal component of the current. Since the latter is not important for the longitudinal hydrodynamic transport, there is no need to specify the explicit form of the transfer term $Q_s^{(\text{FA})}$. Therefore, the steady longitudinal flow in the bulk is described by the following equation:

$$\eta \partial_y^2 u_x(y) - enE_x - \frac{w}{v_F^2 \tau} u_x(y) = 0. \quad (23)$$

Here, as in Ref. [44], we omitted ∇P in the flow equation. In view of the slab's geometry, there is no dependence on x and z . Then, the general solution to Eq. (23) reads

$$u_x(y) = C_1 e^{\lambda_x y} + C_2 e^{-\lambda_x y} - \frac{env_F^2 \tau E_x}{w}, \quad (24)$$

where

$$\lambda_x = \sqrt{\frac{w}{\eta v_F^2 \tau}} \quad (25)$$

and the constants C_1 and C_2 are determined from the BCs. In particular, the condition in Eq. (13) takes the form

$$s\eta \partial_y u_x(y_s) = u_x(y_s) \frac{\alpha w}{v_F} \left[1 - \frac{w^{(\text{FA})}}{v_F \tau_{sb}} \left(\text{sen}^{(\text{FA})} E_x + \frac{w^{(\text{FA})}}{v_F \tau_{sb}} \right)^{-1} \right] + \frac{en^{(\text{FA})} E_x w^{(\text{FA})}}{v_F \tau_{sb}} \left(\text{sen}^{(\text{FA})} E_x + \frac{w^{(\text{FA})}}{v_F \tau_{sb}} \right)^{-1}, \quad (26)$$

where we used the following expression for $u_x^{(\text{FA})}$ obtained from Eqs. (5) and (22):

$$u_x^{(\text{FA})}(y_s) = - \left(v_F en^{(\text{FA})} E_x - \alpha w u_x(y_s) \right) \left(\text{sen}^{(\text{FA})} E_x + \frac{w^{(\text{FA})}}{v_F \tau_{sb}} \right)^{-1}. \quad (27)$$

It is instructive to consider the following two limiting cases: (i) no transfer of electrons from the surface to the bulk $\tau_{sb} \rightarrow \infty$ and (ii) a very strong outflow from the surface to the bulk $\tau_{sb} \rightarrow 0$.

In the absence of electron transfer between the surface and the bulk ($\tau_{sb} \rightarrow \infty$), we have

$$u_x^{(\text{FA})}(y_s) = -sv_F + s \frac{\alpha w u_x(y_s)}{en^{(\text{FA})} E_x}, \quad (28)$$

$$s\eta \partial_y u_x(y_s) = \frac{\alpha w u_x(y_s)}{v_F}. \quad (29)$$

By noting that the velocity of the Fermi arcs might be as large as v_F , we could argue that the realization of the hydrodynamic regime for the surface quasiparticles is unlikely at large τ_{sb} . Also, in the limit $\alpha \rightarrow 0$, i.e., when the Fermi arcs completely decouple, the BCs in Eq. (29) reduce to the usual free-surface ones and $u_x^{(\text{FA})}(y_s) = -sv_F$.

In the opposite limit, i.e., $\tau_{sb} \rightarrow 0$, we obtain

$$u_x^{(\text{FA})} = 0, \quad (30)$$

$$s\eta\partial_y u_x(y_s) = en^{(\text{FA})}E_x. \quad (31)$$

In this case, there is a strong coupling between the surface and bulk fluids leading to the vanishing Fermi arc fluid velocity. In addition, the boundary conditions for the bulk fluid are modified significantly and are affected by the electric field and the chiral shift.

In a general case, the expression for the fluid velocity in the bulk of a Weyl semimetal can be obtained in an analytical form by using the general solution in Eq. (24) and the BC in Eq. (26). The corresponding expression is, however, rather cumbersome and not very informative. Therefore, instead of presenting it here, we illustrate the key features of the flow, as well as the nontrivial effects of the Fermi arcs by using a representative set of model parameters.

In the analysis, we use the following material constants:

$$v_F = 1.4 \times 10^7 \text{ cm/s}, \quad b = 3 \text{ nm}^{-1}, \quad \tau = 3 \times 10^{-10} \text{ s}, \quad \varepsilon_e = 13, \quad (32)$$

which are comparable to those in Refs. [42, 66–68]. (Note that the estimate for the electric permittivity ε_e is based on the dielectric constants of tungsten [69] and phosphorus [70].) By default, we also use the following values of other model parameters:

$$\mu = 25 \text{ meV}, \quad T = 10 \text{ K}, \quad E_x = 1 \text{ V/m}, \quad L_{y,0} = 10 \mu\text{m}, \quad \tau_{sb} = 1 \text{ ns}, \quad \alpha = 10^{-4}. \quad (33)$$

In order to better understand the role of the surface states, we start with the benchmark results for the case without the Fermi arcs on the surfaces of the slab. Such a situation is realized naturally when the chiral shift is absent (e.g., in Dirac semimetals) or when its direction is perpendicular to the surfaces. In this special case, the bulk fluid velocity in a Weyl semimetal slab is given by [44]

$$u_x(y) = -\frac{v_F^2 \tau e n E_x}{w} \left(1 - \delta \frac{\cosh(\lambda_x y - \lambda_x L_y/2)}{\cosh(\lambda_x L_y/2)} \right), \quad (34)$$

where $\delta = 1$ and $\delta = 0$ correspond to the standard no-slip and free-surface BCs given in Eqs. (15) and (16), respectively. The corresponding profile of the longitudinal bulk flow velocity as a function of the y coordinate is shown in the left panel of Fig. 1. Additionally, in the right panel of Fig. 1, we show the dependence of the flow velocity integrated over the channel width, i.e., $U_x = \int_0^{L_y} u_x(y) dy$, on the slab width L_y .

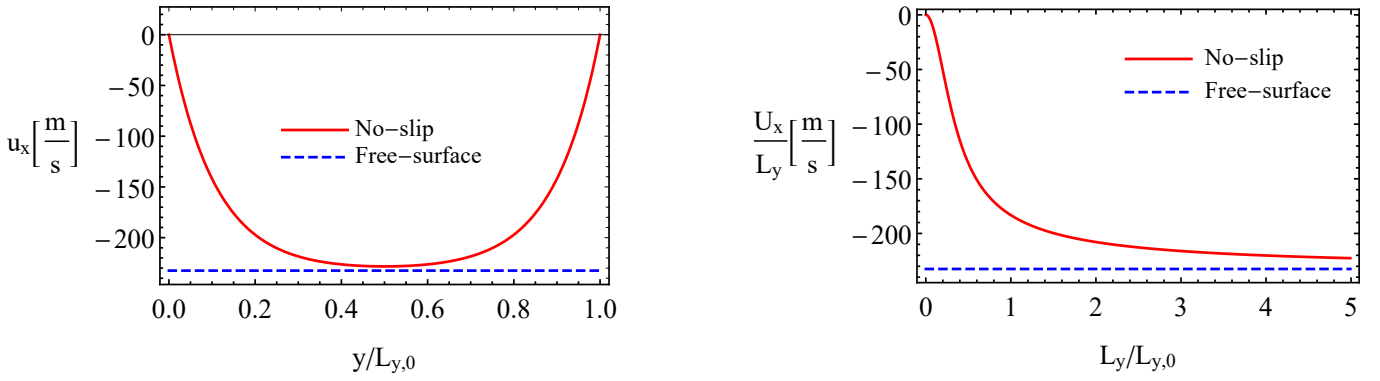


FIG. 1: The longitudinal flow velocity u_x as a function of y (left panel) and the longitudinal flow velocity integrated over the channel width, $U_x = \int_0^{L_y} u_x(y) dy$, as a function of the slab width (right panel). Red solid and blue dashed lines correspond to the standard no-slip (15) and free-surface (16) BCs, respectively.

Now, let us discuss the case of hydrodynamic flow with Fermi arcs on the surfaces. The longitudinal flow velocity u_x and the flow velocity integrated over the channel width U_x for a few values of the coupling parameter α are shown in the left and right panels of Fig. 2, respectively. As we see, the presence of the Fermi arcs enhances the fluid velocity near the boundaries when τ_{sb} is sufficiently small and the transitions from the bulk to the surface, quantified by α , are weak. This is in a drastic contrast to the case of the conventional no-slip or free surface BCs presented in Fig. 1.

The increase of both the fluid velocity and the integrated fluid flow is caused by the Fermi arc fluid that tends to push the bulk one near the surfaces. As expected, the net enhancement of the flow is noticeable only for sufficiently small widths of the slab. It is interesting to note that the fluid velocity profile is rather sensitive to the value of α , which parameterizes the rate of transitions from the bulk to the surface. At the same time, the dependence of U_x on α is very weak. We checked that, with increasing τ_{sb} and/or α , the effect of the Fermi arcs on the bulk hydrodynamic flow weakens and gradually changes to a suppression of the flow velocity near the surfaces. It should be noted that, as expected on the basis of Eq. (28), the Fermi arc fluid velocity also grows with τ_{sb} and could eventually reach large enough values so that the hydrodynamic approach for the surface states becomes unreliable. Therefore, τ_{sb} should remain sufficiently small to allow for the Fermi arcs hydrodynamics.

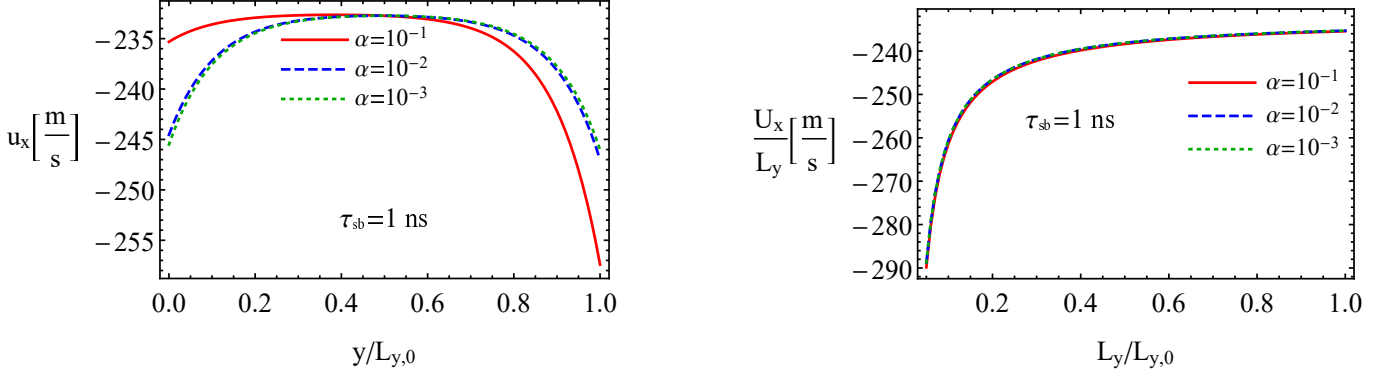


FIG. 2: The longitudinal flow velocity u_x as a function of the y coordinate (left panel) and the longitudinal flow velocity integrated over the channel width, $U_x = \int_0^{L_y} u_x(y) dy$, as a function of the slab width (right panel) for a few fixed values of α . To obtain the numerical results, we used the BC in Eq. (26) and set $\tau_{sb} = 1 \text{ ns}$.

IV. SURFACE COLLECTIVE MODES

In this section, we study the effect of the Fermi arcs on the collective modes in a semi-infinite Weyl semimetal in the hydrodynamic regime. In particular, we focus on the surface plasmons. For simplicity, we assume that the Weyl semimetal is located in the upper half-space ($y > 0$) and the vacuum in the lower half ($y < 0$). Therefore, in the notation of Sec. II, $s = +$. Henceforth, for simplicity, we omit the corresponding subscript in the Fermi arc variables.

Previously, the Fermi arc plasmons have been already studied in Refs. [34–36]. While Ref. [34] employs a simple phenomenological model, the authors of [35] provide a more rigorous quantum-mechanical non-local approach. In this study, by following the approach similar to that used in Refs. [47, 71, 72], we employ the hydrodynamic approximation without the retardation effects in Maxwell’s equations. In this case, the oscillating electric field is governed by the Gauss law

$$\nabla \cdot \delta \mathbf{E}(t, \mathbf{r}) = -\frac{4\pi e}{\varepsilon_e(y)} \delta n(t, \mathbf{r}), \quad (35)$$

or, equivalently, by Poisson’s equation

$$\Delta \phi(t, \mathbf{r}) = \frac{4\pi e}{\varepsilon_e(y)} \delta n(t, \mathbf{r}), \quad (36)$$

where $\delta \mathbf{E}(t, \mathbf{r}) = -\nabla \phi(t, \mathbf{r})$, $\delta n(t, \mathbf{r})$ describes the deviations of the electric charge density from its equilibrium value, $\varepsilon_e(y) = \theta(y)\varepsilon_e + \theta(-y)$ is the electric permittivity of the system, and $\theta(y)$ is the Heaviside step function. The omission of the retardation effects is formally equivalent to setting $c \rightarrow \infty$, which implies that the effects of oscillating magnetic fields can be neglected as well.

By taking into account that the sought collective modes are localized on the surface of a Weyl semimetal, we look for the solutions in the form of plain waves, $\delta X(t, \mathbf{r}) = \delta X(y) e^{-i\omega t + i\mathbf{k}_\perp \cdot \mathbf{r}_\perp}$, where ω is the frequency, $\mathbf{k}_\perp = \{k_x, 0, k_z\}$ is the surface wave vector, and δX is an oscillating hydrodynamic variable, e.g., $\delta \mu$, whose amplitude may depend on the y coordinate.

Following the arguments in Refs. [47, 71, 72], we can neglect the effects of the energy conservation relation and set $\delta T = 0$. Then, all oscillating thermodynamical variables can be expressed in terms of the electric charge density

$$\delta P = \tilde{P} \delta n, \quad (37)$$

$$\delta w = \tilde{w} \delta n, \quad (38)$$

$$\delta w^{(\text{FA})} = \tilde{w}^{(\text{FA})} \delta n^{(\text{FA})}, \quad (39)$$

where

$$\tilde{P} = \frac{\partial P}{\partial \mu} \left(\frac{\partial n}{\partial \mu} \right)^{-1} = \mu \frac{\mu^2 + \pi^2 T^2}{3\mu^2 + \pi^2 T^2} \xrightarrow{T \rightarrow 0} \frac{\mu}{3}, \quad (40)$$

$$\tilde{w} = \frac{\partial w}{\partial \mu} \left(\frac{\partial n}{\partial \mu} \right)^{-1} = 4\mu \frac{\mu^2 + \pi^2 T^2}{3\mu^2 + \pi^2 T^2} \xrightarrow{T \rightarrow 0} \frac{4\mu}{3}, \quad (41)$$

$$\tilde{w}^{(\text{FA})} = \frac{\partial w^{(\text{FA})}}{\partial \mu} \left(\frac{\partial n^{(\text{FA})}}{\partial \mu} \right)^{-1} = \mu. \quad (42)$$

Furthermore, by assuming a gradient flow, which is consistent with the omission of vorticity, the oscillations of the flow velocity can be expressed in terms of the velocity potential $\psi(t, \mathbf{r})$ as follows:

$$\delta \mathbf{u}(t, \mathbf{r}) = -\nabla \psi(t, \mathbf{r}). \quad (43)$$

Then, the Navier-Stokes equation (8), where the surface-bulk transitions are accounted for by the BCs, takes the form

$$i\omega \frac{w}{v_F^2} \nabla \psi + \tilde{P} \nabla \delta n + \left(\zeta + \frac{4}{3} \eta \right) \Delta \nabla \psi - en \nabla \phi - \frac{w}{v_F^2 \tau} \nabla \psi = 0. \quad (44)$$

By using the continuity relation (18), the oscillating electric charge density can be reexpressed via the fluid velocity and electric potentials as follows:

$$-i\omega \delta n - n \Delta \psi + \frac{\sigma}{e} \Delta \phi = 0 \quad \rightarrow \quad \delta n = \frac{in}{\omega} \Delta \psi - \frac{i\sigma}{\omega e} \Delta \phi. \quad (45)$$

This implies that the Poisson equation (36) inside the semimetal takes the form

$$\Delta \phi = i \frac{4\pi en}{\varepsilon_e \omega \tilde{\sigma}} \Delta \psi, \quad (46)$$

where $\tilde{\sigma} = \left(1 + i \frac{4\pi\sigma}{\varepsilon_e \omega} \right)$. By making use of the last two equations, we can rewrite the Navier-Stokes equation (44) as

$$\Delta \left[\omega^2 \frac{w}{v_F^2} + \frac{\tilde{P}n}{\tilde{\sigma}} \Delta - i\omega \left(\zeta + \frac{4}{3} \eta \right) \Delta - \frac{4\pi e^2 n^2}{\varepsilon_e \tilde{\sigma}} + i\omega \frac{w}{v_F^2 \tau} \right] \psi = 0. \quad (47)$$

As is clear, the solution for ψ that decreases in the bulk of the semimetal has the following form:

$$\psi(y) = C_0^\psi e^{-k_\perp y} + \sum_{j=\pm} C_j^\psi e^{-\lambda_j y}, \quad (48)$$

where λ_j are the roots of the equation

$$\omega^2 \frac{w}{v_F^2} + \frac{\tilde{P}n}{\tilde{\sigma}} (\lambda^2 - k_\perp^2) - i\omega \left(\zeta + \frac{4}{3} \eta \right) (\lambda^2 - k_\perp^2) - \frac{4\pi e^2 n^2}{\varepsilon_e \tilde{\sigma}} \left(1 + i \frac{4\pi\sigma}{\varepsilon_e \omega} \right)^{-1} + i\omega \frac{w}{v_F^2 \tau} = 0, \quad (49)$$

with a positive real part. When λ_j are imaginary, the corresponding modes are hybridized surface-bulk excitations. The solutions to Eq. (49) are given by

$$\lambda_\pm = \pm \frac{\sqrt{3\omega_p^2 + k_\perp^2 (3K^2 - 4iv_F^2 \eta \tilde{\sigma} \omega / w) - 3\omega \tilde{\sigma} (\omega + i/\tau)}}{\sqrt{3K^2 - 4i\eta v_F^2 \tilde{\sigma} \omega / w}}. \quad (50)$$

Here, we used the shorthand notation $K^2 = v_F^2 n \tilde{P} / w$ and introduced the plasma frequency $\omega_p^2 = 4\pi e^2 v_F^2 n^2 / (\varepsilon_e w)$. Note that K^2 approaches $v_F^2/3$ as $T \rightarrow 0$. When the bulk viscosity, dissipation, and the intrinsic conductivity are ignored, the expression in Eq. (50) simplifies down to

$$\lambda_{\pm}^{(0)} = \pm \frac{\sqrt{\omega_p^2 + K^2 k_{\perp}^2 - \omega^2}}{K}. \quad (51)$$

As is clear, only $\lambda_+^{(0)}$ corresponds to a mode localized on the surface.

By using Eqs. (46) and (48), we obtain the expressions for the electric potentials at $y > 0$ (semimetal) and $y < 0$ (vacuum),

$$\phi^{y>0} = C^{\phi} e^{-k_{\perp} y} + i \frac{4\pi e n}{\varepsilon_e \omega} \left(1 + i \frac{4\pi \sigma}{\varepsilon_e \omega} \right)^{-1} \sum_{j=\pm} C_j^{\phi} e^{-\lambda_j y}, \quad (52)$$

$$\phi^{y<0} = \tilde{C}^{\phi} e^{k_{\perp} y}. \quad (53)$$

The oscillating fermion number density δn is then obtained from Eqs. (45), (46), and (48)

$$\delta n = \frac{in}{\omega \tilde{\sigma}} \Delta \psi = \frac{in}{\omega \tilde{\sigma}} \sum_{j=\pm} (\lambda_j^2 - k_{\perp}^2) C_j^{\psi} e^{-\lambda_j y}. \quad (54)$$

Similarly to the fluid flow, the BCs are also important for the surface collective modes. For the oscillating fluid velocity, we impose the same BCs as for the flow in Eqs. (13) and (14), i.e.,

$$\eta \partial_y \delta u_x(0) = ik_x \eta \partial_y \psi(0) = I^{(\text{FA})}, \quad (55)$$

$$\delta u_y(0) = -\partial_y \psi(0) = 0. \quad (56)$$

As is clear from the above equations, the transfer term $I^{(\text{FA})}$ in Eq. (55) should be set to zero.

The BCs for the electric potential follow from the continuity relations. As is easy to see, they take the following form:

$$\phi^{y>0}(0) = \phi^{y<0}(0), \quad (57)$$

$$\varepsilon_e \partial_y \phi^{y>0}(0) - \partial_y \phi^{y<0}(0) = 4\pi e \delta n^{(\text{FA})}. \quad (58)$$

As follows from the last equation, the normal component of the electric field has a jump connected with the singular contribution of the Fermi arcs. According to Ref. [47], the bulk states themselves should not induce a localized (singular) surface charge density. The oscillations of the surface fermion number density can be obtained by using Eqs. (17) and (21), i.e.,

$$ie(\omega - v_F k_x) \delta n^{(\text{FA})} = -J_y(0) = \frac{ik_x b e^2 \phi(0)}{2\pi^2 \hbar} + \sigma \partial_y \phi(0), \quad (59)$$

which lead to the following result:

$$\delta n^{(\text{FA})} = \frac{v_F k_x n^{(\text{FA})} e \phi(0)}{\mu(\omega - v_F k_x)} - i \frac{\sigma \partial_y \phi(0)}{e(\omega - v_F k_x)}. \quad (60)$$

For completeness, let us note that the oscillations of the Fermi arc fluid velocity can be obtained from the following Euler equation:

$$-i \frac{(\omega - v_F k_x)}{v_F} \left(\tilde{w}^{(\text{FA})} \delta n^{(\text{FA})} + 2 \frac{w^{(\text{FA})}}{s v_F} \delta u_x^{(\text{FA})} \right) - ik_x n^{(\text{FA})} e \phi = I^{(\text{FA})}, \quad (61)$$

where $\delta n^{(\text{FA})}$ is given by Eq. (60) and, as follows from Eqs. (55) and (56), $I^{(\text{FA})} = 0$.

Another boundary condition can be derived from the y component of Eq. (44) after expressing $\Delta \psi$ in terms of δn , see Eqs. (45) and (46), as well as utilizing the BC in Eq. (56). Its explicit form reads

$$\left[\tilde{P} - i \frac{\omega \tilde{\sigma}}{n} \left(\zeta + \frac{4}{3} \eta \right) \right] \partial_y \delta n(0) = en \partial_y \phi^{y>0}(0). \quad (62)$$

Equations (56), (57), (58), and (62), are sufficient to reexpress all integration constants in Eqs. (48), (52), and (53) in terms of a single constant that is then fixed by a normalization condition. Also, after satisfying all the boundary conditions, one can determine the dispersion relations for the surface modes. As for the dispersion relations for the hybridized surface-bulk modes, they are obtained from Eq. (49), where λ is a continuous variable [47].

For the sake of simplicity, we neglect the effects of viscosity ($\eta \rightarrow 0$), dissipation ($\tau \rightarrow \infty$), and intrinsic conductivity ($\sigma \rightarrow 0$) in the rest of this section. It is also instructive to start from the benchmark case without the Fermi arcs on the surface of a Weyl semimetal. Then, after satisfying all BCs, Eq. (62) gives the following relation for the modes localized on the surface:

$$K^2 \lambda_+^{(0)} \left(\lambda_+^{(0)} + k_\perp \right) = \frac{\omega_p^2}{1 + \varepsilon_e}, \quad (63)$$

where K and ω_p are defined after Eq. (50). The corresponding positive solution is given by

$$\omega = \frac{1}{\sqrt{2}} \left(\frac{2\varepsilon_e \omega_p^2}{1 + \varepsilon_e} + K^2 k_\perp^2 + K k_\perp \sqrt{\frac{4\omega_p^2}{1 + \varepsilon_e} + K^2 k_\perp^2} \right)^{1/2} \approx \frac{\omega_p \sqrt{\varepsilon_e}}{\sqrt{1 + \varepsilon_e}} + \frac{K k_\perp}{2\sqrt{\varepsilon_e}} + \frac{K^2 k_\perp^2 \sqrt{1 + \varepsilon_e} (2\varepsilon_e - 1)}{8\omega_p \varepsilon_e^{3/2}} + O(k_\perp^3). \quad (64)$$

Note that the long-wavelength approximation is well defined and consistent with the nonretarded regime, only at $\omega < ck_\perp$. By taking into account the large value of c , the range of validity of the above result extends to rather small values of the wave vector, $k_\perp \simeq \omega_p/c$. The surface plasmon frequency ω in Eq. (64) qualitatively agrees with the results obtained in Refs. [47, 71, 72]. As we see, the spectrum of the surface plasmons is isotropic and has a nonzero gap. Moreover, the value of the gap agrees with that obtained in Ref. [73] after one sets $\varepsilon_e = 1$.

Now let us analyze the effect of the Fermi arcs on the surface collective modes. Because of a nonzero surface charge density in Eq. (58), the characteristic equation becomes more complicated

$$K^2 \lambda_+^{(0)} (k_\perp + \lambda_+^{(0)}) = \frac{\omega_p^2 [\omega_b + (\omega - v_F k_x)]}{\omega_b + (1 + \varepsilon_e)(\omega - v_F k_x)}, \quad (65)$$

where we introduced the following shorthand notation for the term proportional to the chiral shift b :

$$\omega_b = \frac{k_x}{k_\perp} \frac{4\pi v_F e^2 n^{(\text{FA})}}{\mu} = \frac{k_x}{k_\perp} \frac{2e^2 b}{\pi \hbar}. \quad (66)$$

By solving the characteristic equation to the leading order in the wave vector, we obtain the following dispersion relations:

$$\omega_\pm = \frac{1}{2(1 + \varepsilon_e)} \left(-\omega_b \pm \sqrt{\omega_b^2 + 4\varepsilon_e(1 + \varepsilon_e)\omega_p^2} \right) + O(k_\perp), \quad (67)$$

$$\omega^{(\text{FA})} = v_F k_x - \frac{k_\perp K \omega_b}{\varepsilon_e \omega_p} + O(k_\perp^2). \quad (68)$$

The modes with ω_\pm can be identified with the surface plasmons. Their frequencies are similar to those in Eq. (16) of Ref. [35]. It can be also verified that, in agreement with the analysis in Ref. [34], the dispersion relations in Eq. (67) have discontinuities $\propto \text{sign}(k_x)$ at $k_x = 0$, namely $(\lim_{k_x \rightarrow +0} - \lim_{k_x \rightarrow -0}) \lim_{k_z \rightarrow 0} \omega_\pm = -|\omega_b|/(1 + \varepsilon_e)$. Such discontinuities disappear at $k_z \neq 0$. It is important to note that, depending on the chiral shift, ω_+ (ω_-) at $k_x < 0$ ($k_x > 0$) could be significantly larger than $\omega_p^2 + K^2 k_\perp^2$. Then, by taking into account that the characteristic root defined in Eq. (51) becomes purely imaginary, the corresponding excitations should be identified with the hybridized surface-bulk modes [47, 72] and, henceforth, will be omitted.

In contrast to the surface plasmons, which exist even in the absence of the Fermi arcs, the mode with the dispersion relation in Eq. (68) originates exclusively from the surface states. It is somewhat reminiscent of the usual surface acoustic plasmon [48] with a linear dispersion relation. However, the new mode stemming from the Fermi arcs has a rather unconventional directional dependence.

The frequencies of the surface plasmons and the Fermi arc mode are presented in Figs. 3 and 4 for two different values of the chiral shift, namely $b = 3 \text{ nm}^{-1}$ and $b = 0.3 \text{ nm}^{-1}$, respectively. In both figures, the solid and dashed lines correspond to the numerical solutions of Eq. (65) and the approximate results in Eqs. (67) and (68), respectively. Black dots indicate the frequencies at which the surface modes hybridize with the bulk ones. In agreement with the previous analysis in Ref. [34], we found three roots of the characteristic equation (65). Two of them correspond to ω_\pm in Eq. (67), which are related by the transformation $\omega \rightarrow -\omega$ and $\mathbf{k}_\perp \rightarrow -\mathbf{k}_\perp$ (the modes with $\omega < 0$ are not

shown in the figures). The third solution describes a gapless Fermi arc surface mode with the dispersion relation that, at leading order in small \mathbf{k}_\perp , is approximately given by Eq. (68). It is interesting that, while the surface plasmon does not qualitatively change with the decreasing chiral shift, the corresponding effect is more radical for the gapless mode, where the frequency gradually reduces to just the first term in Eq. (68). As one can see from Figs. 3 and 4, the leading order approximate expressions (67) and (68) describe the collective modes rather well only when either the chiral shift or the wave vector is sufficiently small.

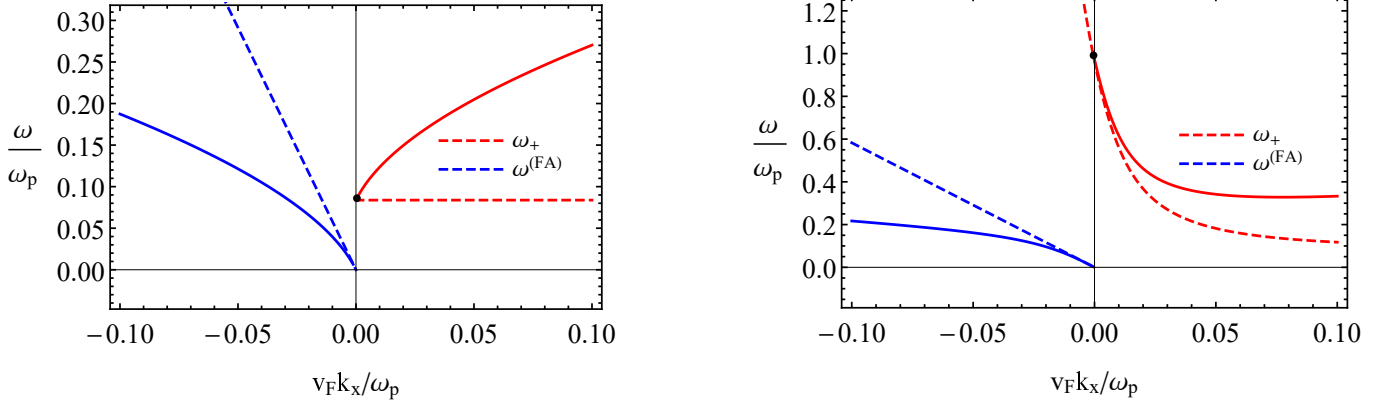


FIG. 3: The solutions for the surface collective modes in the presence of the Fermi arcs. Solid and dashed lines correspond to the exact solutions of the characteristic equation and the approximate ones in Eqs. (67) and (68), respectively. The red lines correspond to the gapped surface plasmons and the blue lines describe the Fermi arc surface mode. Left and right panels show the results for $k_z = 0$ and $k_z = 0.1 \omega_p/v_F$. Black dots indicate the frequencies at which the surface modes hybridize with the bulk ones. The value of the chiral shift is $b = 3 \text{ nm}^{-1}$.

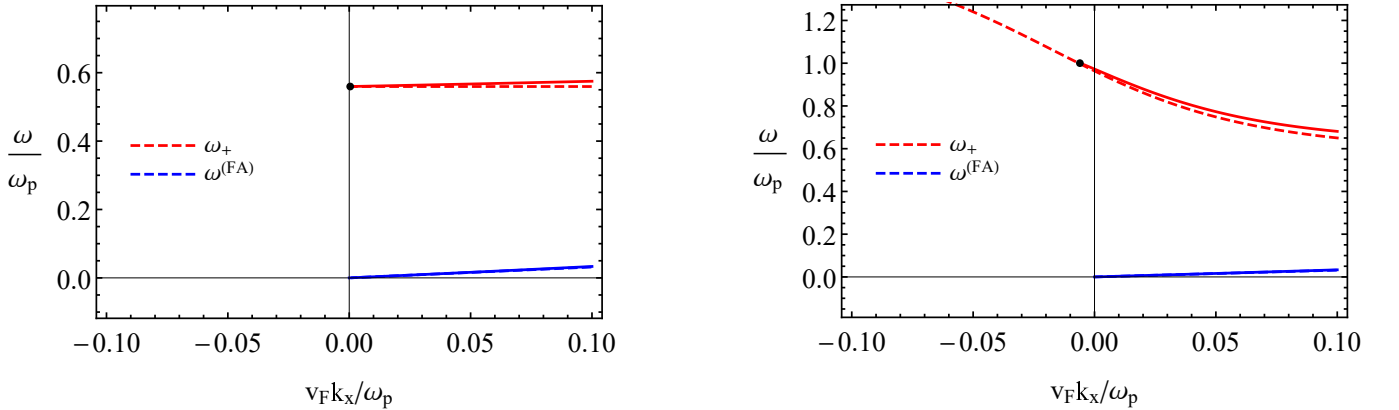


FIG. 4: The solutions for the surface collective modes in the presence of the Fermi arcs. Solid and dashed lines correspond to the exact solutions of the characteristic equation and the approximate ones in Eqs. (67) and (68), respectively. The red lines correspond to the gapped surface plasmons and the blue lines describe the Fermi arc surface mode. Left and right panels show the results for $k_z = 0$ and $k_z = 0.1 \omega_p/v_F$. Black dots indicate the frequencies at which the surface modes hybridize with the bulk ones. The value of the chiral shift is $b = 0.3 \text{ nm}^{-1}$.

In order to clarify the dependence of the surface mode frequencies on the wave vectors, we present the contour plots for the positive frequency plasmon and the Fermi arc surface mode in Figs. 5 and 6 for two different values of the chiral shift. As one can see from the left panel of Fig. 5, for a large value of the chiral shift given in Eq. (32), the contour lines of the gapped surface plasmon are closed ellipses elongated in the direction of the Fermi arcs, i.e., k_x . The contours of the Fermi arc mode are bell-shaped that, with increasing the momenta, gradually become parallel to k_z . When the chiral shift is small and the rate of surface-bulk transitions is high, the contour lines for the gapped mode are strongly elongated and those for the gapless mode become almost parallel to k_z , see Fig. 6. It is fair to say, however, that the change of the plasmon mode with the chiral shift is quantitative rather than qualitative.

By noting that the group velocities of the surface collective modes are given by the derivatives of their frequencies

with respect to momenta, they can be represented by the vectors normal to the contour lines. Then, as is clear from Figs. 5 and 6, the surface plasmon waves tend to spread and propagate primarily parallel to k_x . When the chiral shift is large enough, however, the surface plasmons could also propagate radially similarly to the conventional surface plasmons with the frequency in Eq. (64). The gapless modes, on the other hand, always propagate in one direction, although there is a noticeable spreading at a large chiral shift. Interestingly, the direction of the propagation can be switched with changing the value of the chiral shift, as was already evident from Figs. 5 and 6.

It should be emphasized that the constant-frequency contours for the plasmon modes obtained in this study are closed ellipses. This may appear to be qualitatively different from the open hyperbolic contours in Refs. [34, 35]. We checked, however, that in the hydrodynamic approximation the latter correspond to the hybridized surface-bulk modes with large frequencies. In addition, the open contours at large enough negative k_x (or q_y in the notation of Ref. [35]) in Fig. 2(a) of Ref. [35] could, presumably, stem from the hybridization of the gapped and gapless modes.

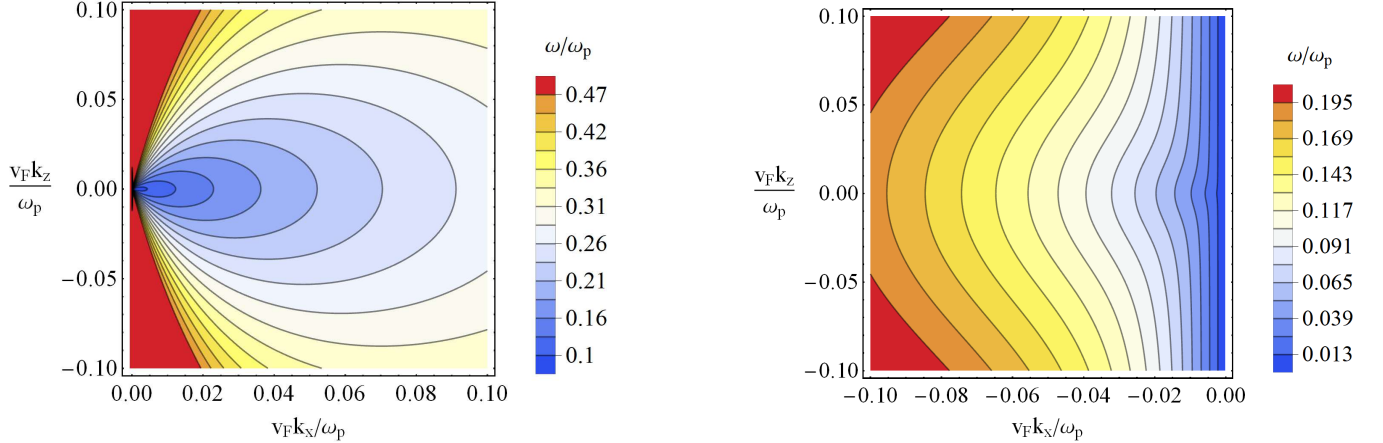


FIG. 5: The contour plots for the surface plasmon (left panel) and the Fermi arc mode (right panel) frequencies. The group velocity is normal to the contour lines and only the results for $\omega > 0$ are presented. Note that the distortions at very small k_x and k_z are numerical artifacts. The value of the chiral shift is $b = 3 \text{ nm}^{-1}$.

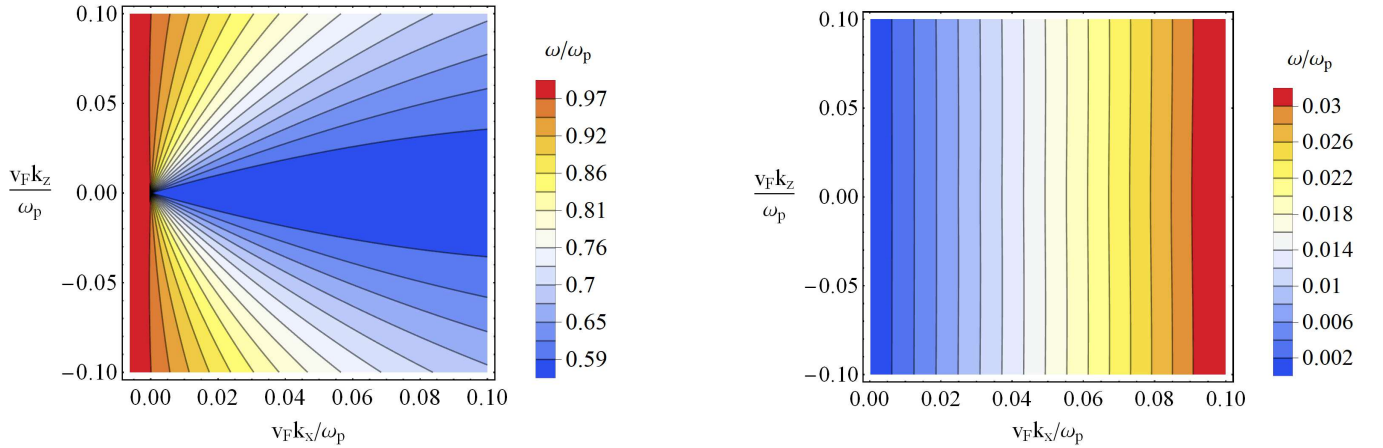


FIG. 6: The contour plots for the surface plasmon (left panel) and the Fermi arc mode (right panel) frequencies. The group velocity is normal to the contour lines and only the results for $\omega > 0$ are presented. Note that the distortions at very small k_x and k_z are numerical artifacts. The value of the chiral shift is $b = 0.3 \text{ nm}^{-1}$.

In general, we identify two qualitative features that could be used to analyze the effects of the Fermi arcs on the surface collective modes in Weyl semimetals. First of all, unlike the conventional surface plasmons with the frequency given in Eq. (64), the Fermi arc surface plasmons are described by a strongly anisotropic dispersion relation. Also, unlike the gapped plasmon mode, which exists even in the absence of the surface Fermi arc states, the new gapless collective mode appears only when the topological surface states are taken into account. Therefore, if experimentally

observed, the latter wave can be used to extract the information about the separation between the Weyl nodes as well as the dispersion relation of the Fermi arcs.

Experimentally, the anisotropy induced by the surface states can be probed using the near-field optical spectroscopy (for a review, see Ref. [37]), as well as the momentum-resolved electron energy loss spectroscopy (see, e.g., Ref. [38]). Because of a possible interference between the surface modes from different pairs of Weyl nodes [34], the most suitable materials are the Weyl semimetals with a single pair of nodes. Therefore, the magnetic Heusler compounds with a broken TR symmetry [74, 75] might be promising candidates for the study of the surface collective modes.

V. SUMMARY

In this paper, we proposed that the Weyl semimetals with a broken TR symmetry may allow a hydrodynamic regime with a nontrivial interplay of the bulk electron fluid and the fluid formed by the surface Fermi arc quasiparticles. The hydrodynamic equations for the latter are derived from the kinetic theory under the assumptions that the electron-electron scattering rate dominates over the electron-impurity and electron-phonon ones. Further, we considered only the case where the hydrodynamic regime is achieved for both surface and bulk quasiparticles of the semimetal. In principle, however, the regime where the electron fluid is formed only on the surface but not in the bulk could be also possible. Such a scenario is likely to lead to unique features and deserves a separate study.

In the proposed two-fluid framework, we studied the role of the Fermi arc fluid on the bulk flow and on the spectrum of surface collective modes. For simplicity, we assumed that the surface fluid is inviscid and couples to the bulk via the phenomenological inflow and outflow terms. The latter describe the Fermi arc dissipation into the bulk and the transitions from the bulk to the surface states. We found that the Fermi arcs modify the boundary conditions for the bulk electron fluid. Depending on the rate of the surface-bulk transitions as well as the value of the chiral shift, the bulk fluid velocity could change noticeably near the boundaries. When the electrons are transferred to the surface at a greater rate than to the bulk, the bulk fluid could be dragged by the surface one. Such a regime, however, is characterized by large surface flow velocities at which the hydrodynamic description may become ill-defined. On the other hand, an unconventional increase of the bulk fluid flow near the boundaries is seen when the surface to bulk transitions dominate. Such a manifestation of the Fermi arc flow could be, in principle, observed via the decrease of the resistivity in samples of small width.

In this study, we also demonstrated that the Fermi arcs profoundly affect the surface collective modes in the hydrodynamic regime. In particular, we found that the dispersion relations of the surface plasmons become anisotropic in the momentum space. This is in contrast to the conventional surface plasmons with the isotropic dispersion. The origin of the anisotropy is the dispersion relation of the surface Fermi arc quasiparticles. In general, we identified two types of surface modes. While one of them is a gapped surface plasmon slightly hybridized with the Fermi arc oscillations, the other is a gapless mode triggered exclusively by the surface states. Similarly to the usual surface acoustic plasmons [48], the gapless Fermi arc mode has a linear dispersion relation, but it is sensitive to the sign of the wave vector component along the direction of the Fermi arc velocity. While our results agree qualitatively with those in Refs. [34, 35], we argue that the only true surface plasmon modes are those with the closed elliptic contours of constant frequency.

In passing, let us discuss a few limitations of this study. The hydrodynamic model proposed in this paper is phenomenological and the underlying reasons for the fluid formation should be rigorously clarified. In our analysis, we used a simplified model for the Fermi arcs without any curvature. While we believe that the results will remain qualitatively the same for slightly curved arcs, the precise role of a nonzero curvature should be addressed in the future. In our study of the surface collective modes, we also neglected the viscosity and dissipation effects, which could be rigorously taken into account via nonlocal corrections as in Ref. [35]. In future investigations, it will be interesting to address also the effects of multiple pairs of Weyl nodes and, thus, multiple components of the surface fluids of Fermi arcs. It is reasonable to suggest that the corresponding results will be rather involved due to a complicated interference of individual components. Such an investigation is beyond the scope of this study, but it should be addressed in the future studies.

Acknowledgments

The work of E.V.G. was partially supported by the Program of Fundamental Research of the Physics and Astronomy Division of the National Academy of Sciences of Ukraine. The work of V.A.M. and P.O.S. was supported by the Natural Sciences and Engineering Research Council of Canada. The work of I.A.S. was supported by the U.S. National Science Foundation under Grant PHY-1713950. P.O.S. is grateful for the hospitality of Nordita during the program “Quantum

Anomalies and Chiral Magnetic Phenomena”, where a part of the study was done, as well as appreciates the discussion with Prof. V. Juričić at the initial stage of the project.

Appendix A: Derivation of the Fermi arc hydrodynamics

In this appendix, we present the technical details of derivation of the hydrodynamic equation for the Fermi arc surface states. We utilize a simple model of a time-reversal symmetry breaking Weyl semimetal with two Weyl nodes separated in momentum space by $2b$ along the z direction, where b is the magnitude of the chiral shift. The semimetal is finite along the y direction and infinite in the other two.

1. Kinetic theory

In our derivation, we follow the standard approach [49, 50] of obtaining the hydrodynamic equation from the kinetic theory. In the presence of an electric field \mathbf{E} , the kinetic equation reads

$$\partial_t f^{(\text{FA})} - e\mathbf{E} \cdot \partial_{\mathbf{p}} f^{(\text{FA})} + \mathbf{v}_p^{(\text{FA})} \cdot \nabla f^{(\text{FA})} = I_{\text{coll}}^{(\text{FA})}, \quad (\text{A1})$$

where $-e$ is the electron charge, $\mathbf{p} = (p_x, p_z)$ is the momentum of the surface quasiparticles and $I_{\text{coll}}^{(\text{FA})}$ denotes the collision integral, whose explicit form will be discussed latter.

Since hydrodynamics assumes a local equilibrium, we take the distribution function in the following form:

$$f^{(\text{FA})} = \delta(y - y_s) \frac{1}{1 + \exp\left(\frac{\epsilon_p^{(\text{FA})} - (\mathbf{u}^{(\text{FA})} \cdot \mathbf{p}) - \mu}{T}\right)}, \quad (\text{A2})$$

where y_s denotes the surface coordinate, $s = \pm$ denotes the bottom (+) or top (-) surface, $\mathbf{u}^{(\text{FA})}$ is the local fluid velocity of the surface Fermi arc states, μ is the electric chemical potential, and T is temperature. For a slab of finite thickness, $y_- = L_y$ and $y_+ = 0$ denote the top and bottom surfaces, respectively. Here we assume that the Fermi arcs are strongly localized at the surface and the dependence of the distribution function on the transverse coordinate can be modeled by the δ -function.

The quasiparticle energy for the surface states reads

$$\epsilon_p^{(\text{FA})} = s v_F p_x, \quad (\text{A3})$$

where v_F is the Fermi velocity. (For the derivation of the Fermi arcs and their dispersion relation see, e.g., Refs. [10, 24, 25].) The corresponding quasiparticle velocity is given by

$$\mathbf{v}_p^{(\text{FA})} = \partial_{\mathbf{p}} \epsilon_p^{(\text{FA})} = s v_F \hat{\mathbf{x}}, \quad (\text{A4})$$

where $\hat{\mathbf{x}}$ is the unit vector in the x direction. Since the Fermi arc quasiparticles move only along the x axis, it is reasonable to assume that the surface hydrodynamic motion is also possible only along that axis, i.e., $\mathbf{u}^{(\text{FA})} \parallel \hat{\mathbf{x}}$. As we will show in Sec. A 4, this is further justified by the fact that the Fermi arc electric current can only flow along the x direction.

In the case of small fluid velocities, we can use the following expansion for the distribution function:

$$f^{(\text{FA})} \approx f^{(\text{FA},0)} - p_x u_x^{(\text{FA})} \frac{\partial f^{(\text{FA},0)}}{\partial \epsilon_p}, \quad (\text{A5})$$

where

$$f^{(\text{FA},0)} = \delta(y - y_s) \frac{1}{1 + e^{(s v_F p_x - \mu)/T}} \quad (\text{A6})$$

is the distribution function of the Fermi arc quasiparticles in global equilibrium.

2. The Euler equation for the Fermi arc fluid

In order to derive the Euler equation, we multiply Eq. (A1) with the x component of the momentum p_x and integrate over p_x . (It should be noted that, because of the dispersion relation (A3), there is no independent energy conservation equation.)

The integration of the first term in Eq. (A1) leads to the following result:

$$\begin{aligned} \int \frac{d^2p}{(2\pi\hbar)^2} p_x \partial_t f^{(\text{FA})} &= \int \frac{d^2p}{(2\pi\hbar)^2} p_x \partial_t \left(f^{(\text{FA},0)} - p_x u_x^{(\text{FA})} \frac{\partial f^{(\text{FA},0)}}{\partial \epsilon_p} \right) = -\partial_t \sum_{\text{p,a}} \frac{sFT^2}{2\pi v_F^2 \hbar^2} \text{Li}_2 \left(-e^{\mu/T} \right) \\ &\quad - \sum_{\text{p,a}} \partial_t \frac{FT^2 u_x^{(\text{FA})}}{\pi v_F^3 \hbar^2} \left[\frac{\pi^2}{6} - \text{Li}_2 \left(1 + e^{\mu/T} \right) - \left(\frac{\mu}{T} + i\pi \right) \ln \left(1 + e^{\mu/T} \right) \right] \\ &= \partial_t \frac{sF}{4\pi v_F^2 \hbar^2} \left(\mu^2 + \frac{\pi^2 T^2}{3} \right) \left(1 + \frac{2u_x^{(\text{FA})}}{sv_F} \right), \end{aligned} \quad (\text{A7})$$

where we took into account the small fluid velocity expansion in Eq. (A5) and use the formulas in Appendix B. Further, $\sum_{\text{p,a}}$ denotes the summation over particles (electrons) and antiparticles (holes). It should be noted that $\mu \rightarrow -\mu$ and $e \rightarrow -e$ for holes and the limits of integration over p_x depends on the boundary label s , i.e., $\int_0^{s\infty} dp_x$. The overall coefficient F is defined by the integration over the length of the Fermi arc, i.e.,

$$F = \int_{-\hbar b}^{\hbar b} \frac{dp_z}{2\pi} = \frac{\hbar b}{\pi}. \quad (\text{A8})$$

The integral with the term containing the electric field in Eq. (A1) can be calculated in a similar way. The result reads

$$\begin{aligned} -e \int \frac{d^2p}{(2\pi\hbar)^2} p_x (\mathbf{E} \cdot \partial_{\mathbf{p}}) f^{(\text{FA})} &= \sum_{\text{p,a}} \frac{e}{2\pi\hbar^2} \frac{E_x F T}{v_F} \ln \left(1 + e^{\mu/T} \right) + \sum_{\text{p,a}} \frac{se}{2\pi\hbar^2} \frac{u_x^{(\text{FA})} E_x F T}{v_F^2} \ln \left(1 + e^{\mu/T} \right) \\ &= \frac{e E_x F \mu}{2\pi v_F \hbar^2} \left(1 + \frac{u_x^{(\text{FA})}}{sv_F} \right). \end{aligned} \quad (\text{A9})$$

The term with the spatial derivatives gives rise to the following result:

$$\begin{aligned} \int \frac{d^2p}{(2\pi\hbar)^2} p_x (\mathbf{v}_p^{(\text{FA})} \cdot \nabla) f^{(\text{FA})} &= -\sum_{\text{p,a}} sv_F \partial_x \frac{FT^2}{2\pi v_F^2 \hbar^2} \text{Li}_2 \left(-e^{\mu/T} \right) \\ &\quad - \sum_{\text{p,a}} sv_F \partial_x \frac{FT^2 u_x^{(\text{FA})}}{\pi v_F^3 \hbar^2} \left[\frac{\pi^2}{6} - \text{Li}_2 \left(1 + e^{\mu/T} \right) - \left(\frac{\mu}{T} + i\pi \right) \ln \left(1 + e^{\mu/T} \right) \right] \\ &= \partial_x \frac{F}{4\pi v_F \hbar^2} \left(\mu^2 + \frac{\pi^2 T^2}{3} \right) \left(1 + 2 \frac{u_x^{(\text{FA})}}{sv_F} \right). \end{aligned} \quad (\text{A10})$$

By collecting all contributions together, we finally arrive at the following Euler equation for the Fermi arc fluid:

$$(\partial_t + sv_F \partial_x) \frac{sF}{4\pi v_F^2 \hbar^2} \left(\mu^2 + \frac{\pi^2 T^2}{3} \right) \left(1 + 2 \frac{u_x^{(\text{FA})}}{sv_F} \right) + \frac{e\mu F}{2\pi v_F \hbar^2} \left(1 + \frac{u_x^{(\text{FA})}}{sv_F} \right) E_x = I^{(\text{FA})}. \quad (\text{A11})$$

3. The transfer term

Here we present the derivation of the transfer term on the right hand side of the Euler equation (A11). In general, it may contain two different parts: one describing the surface to bulk transitions and the other describing the inflow from the bulk. By recalling that the dissipation of the Fermi arcs is primarily due to the surface to bulk scatterings [25],

the first part of $I^{(\text{FA})}$ can be obtained by using the relaxation time approximation as follows:

$$\begin{aligned}
& - \int \frac{d^2 p}{(2\pi\hbar)^2} p_x \frac{f^{(\text{FA})} - f^{(\text{FA},0)}}{\tau_{sb}} = \int \frac{d^2 p}{(2\pi\hbar)^2} p_x \frac{p_x u_x^{(\text{FA})}}{\tau_{sb}} \frac{\partial f^{(\text{FA},0)}}{\partial \epsilon_p} \\
& = \frac{1}{\tau_{sb}} \sum_{p,a} \frac{FT^2 u_x^{(\text{FA})}}{\pi v_F^3 \hbar^2} \left[\frac{\pi^2}{6} - \text{Li}_2 \left(1 + e^{\mu/T} \right) - \left(\frac{\mu}{T} + i\pi \right) \ln \left(1 + e^{\mu/T} \right) \right] \\
& = - \frac{u_x^{(\text{FA})}}{\tau_{sb}} \frac{F}{2\pi v_F^3 \hbar^2} \left(\mu^2 + \frac{\pi^2 T^2}{3} \right). \tag{A12}
\end{aligned}$$

The term describing the bulk to surface transitions, on the other hand, can be calculated by using the method in the Supplemental Material of Ref. [43]. Its explicit form reads

$$\lambda_B \frac{w u_x(y_s)}{\tau_{bs} v_F^2}, \tag{A13}$$

where $u_x(y_s)$ is the bulk fluid velocity on the surface, w in the bulk enthalpy density, λ_B is the dimensional coefficient, and τ_{bs} is the relaxation time describing bulk to surface transitions. It might be more convenient to parameterize the bulk inflow in terms of a single overall coefficient $\alpha = \lambda_B v_F / \tau_{bs}$. Then, the final expression for the transfer term $I^{(\text{FA})}$ takes the form as in Eq. (22) in the main text.

4. The electric charge and current densities of Fermi arcs

For completeness, here we present the explicit expressions for the electric charge and current densities for Fermi arc quasiparticles. The corresponding expressions can be obtained by using the kinetic theory, i.e.,

$$\begin{aligned}
\rho^{(\text{FA})} &= - \sum_{p,a} e \int \frac{d^2 p}{(2\pi\hbar)^2} f^{(\text{FA})} = - \sum_{p,a} e \int \frac{d^2 p}{(2\pi\hbar)^2} \left[f^{(\text{FA},0)} - p_x u_x^{(\text{FA})} \frac{\partial f^{(\text{FA},0)}}{\partial \epsilon_p} \right] \\
&= - \sum_{p,a} \frac{seF}{2\pi\hbar^2} \left[\frac{T}{sv_F} \ln \left(1 + e^{\mu/T} \right) + u_x^{(\text{FA})} \frac{T}{s^2 v_F^2} \ln \left(1 + e^{\mu/T} \right) \right] = - \frac{e\mu F}{2\pi v_F \hbar^2} \left(1 + \frac{u_x^{(\text{FA})}}{sv_F} \right) \tag{A14}
\end{aligned}$$

and

$$\begin{aligned}
\mathbf{J}^{(\text{FA})} &= - \sum_{p,a} e \int \frac{d^2 p}{(2\pi\hbar)^2} \mathbf{v}_p^{(\text{FA})} f^{(\text{FA})} = - \sum_{p,a} esv_F \hat{\mathbf{x}} \int \frac{d^2 p}{(2\pi\hbar)^2} \left[f^{(\text{FA},0)} - p_x u_x^{(\text{FA})} \frac{\partial f^{(\text{FA},0)}}{\partial \epsilon_p} \right] \\
&= - \sum_{p,a} v_F \hat{\mathbf{x}} \frac{eF}{2\pi\hbar^2} \left[\frac{T}{sv_F} \ln \left(1 + e^{\mu/T} \right) + u_x^{(\text{FA})} \frac{T}{s^2 v_F^2} \ln \left(1 + e^{\mu/T} \right) \right] = -s \hat{\mathbf{x}} \frac{e\mu F}{2\pi\hbar^2} \left(1 + \frac{u_x^{(\text{FA})}}{sv_F} \right), \tag{A15}
\end{aligned}$$

respectively.

Appendix B: Polylogarithm functions

In this appendix, we present several definitions and identities for the polylogarithm functions used in the derivation of the Euler equation. By making use of the short-hand notation $f^{(0)} = 1/[e^{(v_F p - \mu)/T} + 1]$, it is straightforward to derive the following formulas:

$$\int_0^\infty dp p^n f^{(0)} = - \frac{T^{n+1} \Gamma(n+1)}{v_F^{n+1}} \text{Li}_{n+1} \left(-e^{\mu/T} \right), \quad n \geq 0, \tag{B1}$$

$$\int_0^\infty dp p^n \frac{\partial f^{(0)}}{\partial p} = \frac{T^n \Gamma(n+1)}{v_F^n} \text{Li}_n \left(-e^{\mu/T} \right), \quad n \geq 0, \tag{B2}$$

where $\text{Li}_n(x)$ is the polylogarithm function. The polylogarithm functions of order $n = 0$ and $n = 1$ can be expressed in terms of elementary functions, i.e.,

$$\text{Li}_0(-e^x) = -\frac{1}{1 + e^{-x}}, \tag{B3}$$

$$\text{Li}_1(-e^x) = -\ln(1 + e^x). \tag{B4}$$

Also, the following identities are useful

$$\text{Li}_0(-e^x) + \text{Li}_0(-e^{-x}) = -1, \quad (\text{B5})$$

$$\text{Li}_1(-e^x) - \text{Li}_1(-e^{-x}) = -x, \quad (\text{B6})$$

$$\text{Li}_2(-e^x) + \text{Li}_2(-e^{-x}) = -\frac{1}{2} \left(x^2 + \frac{\pi^2}{3} \right), \quad (\text{B7})$$

$$\text{Li}_2(1 + e^x) + \text{Li}_2(1 + e^{-x}) + i\pi [\ln(1 + e^x) + \ln(1 + e^{-x})] = \frac{1}{2} [\pi^2 - \ln^2(e^x)]. \quad (\text{B8})$$

[1] B. Yan and C. Felser, *Annu. Rev. Condens. Matter Phys.* **8**, 337 (2017).

[2] M. Z. Hasan, S.-Y. Xu, I. Belopolski, and C.-M. Huang, *Annu. Rev. Condens. Matter Phys.* **8**, 289 (2017).

[3] N. P. Armitage, E. J. Mele, and A. Vishwanath, *Rev. Mod. Phys.* **90**, 015001 (2018).

[4] M. V. Berry, *Proc. R. Soc. A* **392**, 45 (1984).

[5] H. B. Nielsen and M. Ninomiya, *Nucl. Phys. B* **185**, 20 (1981).

[6] H. B. Nielsen and M. Ninomiya, *Nucl. Phys. B* **193**, 173 (1981).

[7] H. B. Nielsen and M. Ninomiya, *Phys. Lett. B* **130**, 389 (1983).

[8] H. Z. Lu and S. Q. Shen, *Front. Phys.* **12**, 127201 (2017).

[9] S. Wang, B.-C. Lin, A.-Q. Wang, D.-P. Yu, and Z.-M. Liao, *Adv. Phys.: X* **2**, 518 (2017).

[10] E. V. Gorbar, V. A. Miransky, I. A. Shovkovy, and P. O. Sukhachov, *Low Temp. Phys.* **44**, 487 (2018).

[11] X. Wan, A. M. Turner, A. Vishwanath, and S. Y. Savrasov, *Phys. Rev. B* **83**, 205101 (2011).

[12] F. D. M. Haldane, arXiv:1401.0529.

[13] S.-Y. Xu, I. Belopolski, N. Alidoust, M. Neupane, C. Zhang, R. Sankar, S.-M. Huang, C.-C. Lee, G. Chang, B. Wang, G. Bian, H. Zheng, D. S. Sanchez, F. Chou, H. Lin, S. Jia, and M. Z. Hasan, *Science* **349**, 613 (2015).

[14] B. Q. Lv, H. M. Weng, B. B. Fu, X. P. Wang, H. Miao, J. Ma, P. Richard, X. C. Huang, L. X. Zhao, G. F. Chen, Z. Fang, X. Dai, T. Qian, and H. Ding, *Phys. Rev. X* **5**, 031013 (2015).

[15] L. X. Yang, Z. K. Liu, Y. Sun, H. Peng, H. F. Yang, T. Zhang, B. Zhou, Y. Zhang, Y. F. Guo, M. Rahn, D. Prabhakaran, Z. Hussain, S.-K. Mo, C. Felser, B. Yan, and Y. L. Chen, *Nat. Phys.* **11**, 728 (2015).

[16] S.-Y. Xu, N. Alidoust, I. Belopolski, Z. Yuan, G. Bian, T. -R. Chang, H. Zheng, V. N. Strocov, D. S. Sanchez, G. Chang, C. Zhang, D. Mou, Y. Wu, L. Huang, C.-C. Lee, S.-M. Huang, B. Wang, A. Bansil, H.-T. Jeng, T. Neupert, A. Kaminski, H. Lin, S. Jia, and M. Z. Hasan, *Nat. Phys.* **11**, 748 (2015).

[17] S.-Y. Xu, I. Belopolski, D. S. Sanchez, C. Zhang, G. Chang, C. Guo, G. Bian, Z. Yuan, H. Lu, T.-R. Chang, P.P. Shibayev, M. L. Prokopych, N. Alidoust, H. Zheng, C.-C. Lee, S.-M. Huang, R. Sankar, F. Chou, C.-H. Hsu, H.-T. Jeng, A. Bansil, T. Neupert, V. N. Strocov, H. Lin, S. Jia, and M. Z. Hasan, *Sci. Adv.* **1**, e1501092 (2015).

[18] N. Xu, H. M. Weng, B. Q. Lv, C. E. Matt, J. Park, F. Bisti, V. N. Strocov, D. Gawryluk, E. Pomjakushina, K. Conder, N. C. Plumb, M. Radovic, G. Autès, O. V. Yazyev, Z. Fang, X. Dai, T. Qian, J. Mesot, H. Ding, and M. Shi, *Nat. Commun.* **7**, 11006 (2016).

[19] M. Z. Hasan, S.-Y. Xu, I. Belopolski, and S.-M. Huang, *Ann. Rev. of Cond. Mat. Phys.* **8**, 289 (2017).

[20] H. Zheng, S.-Y. Xu, G. Bian, C. Guo, G. Chang, D. S. Sanchez, I. Belopolski, C.-C. Lee, S.-M. Huang, X. Zhang, R. Sankar, N. Alidoust, T.-R. Chang, F. Wu, T. Neupert, F. Chou, H.-T. Jeng, N. Yao, A. Bansil, S. Jia, H. Lin, and M. Z. Hasan, *ACS Nano* **10**, 1378 (2016).

[21] R. Batabyal, N. Morali, N. Avraham, Y. Sun, M. Schmidt, C. Felser, A. Stern, B. Yan, and H. Beidenkopf, *Sci. Adv.* **2**, e1600709 (2016).

[22] H. Inoue, A. Gyenis, Z. Wang, J. Li, S. W. Oh, S. Jiang, N. Ni, B. A. Bernevig, A. Yazdani, *Science* **351**, 1184 (2016).

[23] A. Gyenis, H. Inoue, S. Jeon, B. B. Zhou, B. E. Feldman, Z. Wang, J. Li, S. Jiang, Q. D. Gibson, S. K. Kushwaha, J. W. Krizan, N. Ni, R. J. Cava, B. A. Bernevig, and A. Yazdani, *New J. Phys.* **18**, 105003 (2016).

[24] R. Okugawa and S. Murakami, *Phys. Rev. B* **89**, 235315 (2014).

[25] E. V. Gorbar, V. A. Miransky, I. A. Shovkovy, and P. O. Sukhachov, *Phys. Rev. B* **93**, 235127 (2016).

[26] R. J. Slager, V. Juricic, and B. Roy, *Phys. Rev. B* **96**, 201401 (2017).

[27] J. H. Wilson, J. H. Pixley, D. A. Huse, G. Refael, and S. Das Sarma, *Phys. Rev. B* **97**, 235108 (2018).

[28] F. M. D. Pellegrino, M. I. Katsnelson, and M. Polini, *Phys. Rev. B* **92**, 201407(R) (2015).

[29] J. Hofmann and S. Das Sarma, *Phys. Rev. B* **93**, 241402(R) (2016).

[30] T. Tamaya, T. Kato, S. Konabe, and S. Kawabata, arXiv:1811.08608.

[31] E. V. Gorbar, V. A. Miransky, I. A. Shovkovy, and P. O. Sukhachov, *Phys. Rev. Lett.* **118**, 127601 (2017).

[32] E. V. Gorbar, V. A. Miransky, I. A. Shovkovy, and P. O. Sukhachov, *Phys. Rev. B* **95**, 115202 (2017).

[33] Z. Long, Y. Wang, M. Erukhimova, M. Tokman, and A. Belyanin, *Phys. Rev. Lett.* **120**, 037403 (2018).

[34] J. C. W. Song and M. S. Rudner, *Phys. Rev. B* **96**, 205443 (2017).

[35] G. M. Andolina, F. M. D. Pellegrino, F. H. L. Koppens, and M. Polini, *Phys. Rev. B* **97**, 125431 (2018).

[36] Ž. B. Lošić, *J. Phys.: Condens. Matter* **30**, 365003 (2018).

[37] D. N. Basov, M. M. Fogler, and F. J. García de Abajo, *Science* **354**, 6309 (2016).

- [38] Y. Y. Wang, S. C. Cheng, V. P. Dravid, and F. C. Zhang, *Ultramicroscopy* **59**, 109 (1995).
- [39] G. Chiarello, J. Hofmann, Z. Li, V. Fabio, L. Guo, X. Chen, S. Das Sarma, and A. Politano, arXiv:1811.04639.
- [40] R. N. Gurzhi, *J. Exp. Theor. Phys.* **17**, 521 (1963).
- [41] R. N. Gurzhi, *Sov. Phys. Uspekhi* **11**, 255 (1968).
- [42] J. Gooth, F. Menges, N. Kumar, V. Süß, C. Shekhar, Y. Sun, U. Drechsler, R. Zierold, C. Felser, and B. Gotsmann, *Nat. Commun.* **9**, 4093 (2018).
- [43] E. V. Gorbar, V. A. Miransky, I. A. Shovkovy, and P. O. Sukhachov, *Phys. Rev. B* **97**, 121105(R) (2018).
- [44] E. V. Gorbar, V. A. Miransky, I. A. Shovkovy, and P. O. Sukhachov, *Phys. Rev. B* **97**, 205119 (2018).
- [45] E. V. Gorbar, V. A. Miransky, I. A. Shovkovy, and P. O. Sukhachov, *Phys. Rev. B* **98**, 035121 (2018).
- [46] P. O. Sukhachov, E. V. Gorbar, I. A. Shovkovy, and V. A. Miransky, *J. Phys. Condens. Matter* **30**, 275601 (2018).
- [47] G. Barton, *Rep. Prog. Phys.* **42**, 65 (1979).
- [48] J. M. Pitarke, V. U. Nazarov, V. M. Silkin, E. V. Chulkov, E. Zaremba, and P. M. Echenique, *Phys. Rev. B* **70**, 205403 (2004).
- [49] E. M. Lifshitz and L. P. Pitaevskii, *Physical Kinetics* (Pergamon Press, New York, 1981).
- [50] K. Huang, *Statistical Mechanics* (John Wiley and Sons, New York, 1987).
- [51] A. Lucas, R. A. Davison, and S. Sachdev, *Proc. Natl. Acad. Sci. USA* **113**, 9463 (2016).
- [52] P. S. Alekseev, *Phys. Rev. Lett.* **117**, 166601 (2016).
- [53] L. D. Landau and E. M. Lifshitz, *Fluid Mechanics* (Pergamon, New York, 1959).
- [54] P. Kovtun and A. Ritz, *Phys. Rev. D* **78**, 066009 (2008).
- [55] S. A. Hartnoll, *Nature Phys.* **11**, 54 (2015).
- [56] K. Landsteiner, Y. Liu, and Y. W. Sun, *J. High Energy Phys.* **1503**, 127 (2015).
- [57] R. A. Davison, B. Goutéraux, and S. A. Hartnoll, *J. High Energy Phys.* **1510**, 112 (2015).
- [58] A. Lucas, *New J. Phys.* **17**, 113007 (2015).
- [59] K.-Y. Yang, Y.-M. Lu, and Y. Ran, *Phys. Rev. B* **84**, 075129 (2011).
- [60] A. A. Burkov and L. Balents, *Phys. Rev. Lett.* **107**, 127205 (2011).
- [61] A. A. Burkov, M. D. Hook, and L. Balents, *Phys. Rev. B* **84**, 235126 (2011).
- [62] A. G. Grushin, *Phys. Rev. D* **86**, 045001 (2012).
- [63] A. A. Zyuzin and A. A. Burkov, *Phys. Rev. B* **86**, 115133 (2012).
- [64] P. Goswami and S. Tewari, *Phys. Rev. B* **88**, 245107 (2013).
- [65] A. A. Burkov, *Phys. Rev. Lett.* **113**, 187202 (2014).
- [66] G. Autès, D. Gresch, M. Troyer, A. A. Soluyanov, and O. V. Yazyev, *Phys. Rev. Lett.* **117**, 066402 (2016).
- [67] N. Kumar, Y. Sun, N. Xu, K. Manna, M. Yao, V. Süß, I. Leermakers, O. Young, T. Förster, M. Schmidt, H. Borrmann, B. Yan, U. Zeitler, M. Shi, C. Felser, and C. Shekhar, *Nat. Commun.* **8**, 1642 (2017).
- [68] E. Razzoli, B. Zwartsenberg, M. Michiardi, F. Boschini, R. P. Day, I. S. Elfimov, J. D. Denlinger, V. Süß, C. Felser, and A. Damascelli, *Phys. Rev. B* **97**, 201103(R) (2018).
- [69] M. A. Ordal, R. J. Bell, R. W. Alexander, L. A. Newquist, and M. R. Querry, *Appl. Opt.* **27**, 1203 (1988).
- [70] T. Nagahama, M. Kobayashi, Y. Akahama, S. Endo, and S. Narita, *J. Phys. Soc. Jpn.* **54**, 2096 (1985).
- [71] R. H. Ritchie and R. E. Wilems, *Phys. Rev.* **178**, 372 (1969).
- [72] J. M. Pitarke, V. M. Silkin, E. V. Chulkov, and P. M. Echenique, *Rep. Prog. Phys.* **70**, 1 (2006).
- [73] R. H. Ritchie, *Phys. Rev.* **106**, 874 (1957).
- [74] G. Chang, S.-Y. Xu, H. Zheng, B. Singh, C.-H. Hsu, G. Bian, N. Alidoust, I. Belopolski, D. S. Sanchez, S. Zhang, H. Lin, and M. Z. Hasan, *Sci. Rep.* **6**, 38839 (2016).
- [75] Z. Wang, M. G. Vergniory, S. Kushwaha, M. Hirschberger, E. V. Chulkov, A. Ernst, N. P. Ong, R. J. Cava, and B. A. Bernevig, *Phys. Rev. Lett.* **117**, 236401 (2016).